

Tailoring Slurries Using Cosolvents and Li Salt Targeting Practical All-Solid-State Batteries Employing Sulfide Solid Electrolytes

Kyu Tae Kim, Dae Yang Oh, Seungwoo Jun, Yong Bae Song, Tae Young Kwon, Yoonjae Han, and Yoon Seok Jung*

Polymeric binders that can undergo slurry fabrication and minimize the disruption of interfacial Li^+ contact are imperative for sheet-type electrodes and solid electrolyte films in practical all-solid-state Li batteries (ASLBs). Although dry polymer electrolytes (DPEs) are a plausible alternative, their use is complicated by the severe reactivity of sulfide solid electrolytes and the need to dissolve Li salts. In this study, a new scalable fabrication protocol for a Li^+ -conductive DPE-type binder, nitrile-butadiene rubber (NBR)-LiTFSI, is reported. The less-polar dibromomethane and more-polar hexyl butyrate in cosolvents work synergistically to dissolve NBR and LiTFSI, while preserving $\text{Li}_6\text{PS}_5\text{Cl}_{0.5}\text{Br}_{0.5}$. It is found that the dispersion of NBR can be controlled by the fraction of the antisolvent (hexyl butyrate), which in turn affects the corresponding performance of the ASLBs. Sheet-type $\text{LiNi}_{0.70}\text{Co}_{0.15}\text{Mn}_{0.15}\text{O}_2$ electrodes tailored using NBR-LiTFSI outperform those prepared using the conventional insulating binder (NBR) in terms of capacity (163 vs 147 mA h g^{-1}) and initial Coulombic efficiency (78.9 vs 70.4%), which is attributed to the facilitated interfacial Li^+ transport, as confirmed by ^6Li nuclear magnetic resonance and electrochemical measurements. Moreover, NBR-LiTFSI is functional at 70 °C and in a graphite anode. Finally, the promising performance of pouch-type $\text{LiNi}_{0.70}\text{Co}_{0.15}\text{Mn}_{0.15}\text{O}_2/\text{graphite}$ ASLBs is also demonstrated.

classes of materials, including sulfides (e.g., $\text{Li}_{5.5}\text{PS}_{4.5}\text{Cl}_{1.5}$:^[14,15] $\approx 10 \text{ mS cm}^{-1}$), oxides (e.g., $\text{Li}_7\text{La}_3\text{Zr}_2\text{O}_{12}$:^[16] 0.5 mS cm^{-1}), closo-borates (e.g., $0.7\text{Li}(\text{CB}_9\text{H}_{10})-0.3\text{Li}(\text{CB}_{11}\text{H}_{12})$:^[12,17] 6.7 mS cm^{-1}), and halides (e.g., Li_3YCl_6 :^[18,19] 0.5 mS cm^{-1} , $\text{Li}_{2.25}\text{Zr}_{0.75}\text{Fe}_{0.25}\text{Cl}_6$:^[20] 1 mS cm^{-1}). Furthermore, consideration of multiple aspects, such as mechanical sinterability, cost, and lightness (e.g., $\text{Li}_6\text{PS}_5\text{Cl}$:^[14] 1.86 g cm^{-3} , $\text{Li}_7\text{La}_3\text{Zr}_2\text{O}_{12}$:^[21] 5.11 g cm^{-3} , Li_3YCl_6 :^[18] 2.43 g cm^{-3}), indicates that sulfide materials are highly competitive.^[14,22,23]

To integrate SEs into large-scale ASLBs for mass production, sheet-type electrodes and SE films are required.^[24–33] For this, it is necessary to use soft polymeric binders to avoid delamination and to supplement the brittleness of the inorganic components of the electrode active materials and SEs.^[34–36] Moreover, stresses generated by volumetric strains in electrode active materials upon repeated cycling can be buffered by the polymeric binders.^[34,36,37]


However, the introduction of even a small amount of polymeric binder (e.g., 1–2 wt%) in composite electrodes severely degrades the electrochemical performance of ASLBs (e.g., as much as $\approx 30 \text{ mA h g}^{-1}$ of capacity loss for $\text{LiNi}_{0.6}\text{Co}_{0.2}\text{Mn}_{0.2}\text{O}_2$ electrodes), due to the disruption of interfacial Li^+ contact.^[27,34,38] To address this issue, several approaches have been introduced. Yamamoto and coworkers reported that a binder-free sheet-type battery fabricated using thermally decomposable polymers of poly(propylene carbonate) provided good performance,^[39] but at the expense of the mechanical properties of the battery. Moreover, it was shown that it is possible to use small amounts of binders via a dry process employing a fibrous polytetrafluoroethylene binder.^[40,41] However, a wet-slurry process for ASLBs is still imperative, as it could take advantage of the already-developed manufacturing infrastructure for LIBs.

Recently, our group reported the preparation of Li^+ conductive polymeric binders based on solvate ionic liquids (SILs), which are a solvent-salt complex of Li salt and glyme, such as $\text{Li}(\text{G}3)\text{TFSI}$ ($\text{G}3$: triethylene glycol dimethyl ether, LiTFSI: lithium bis(trifluoromethanesulfonyl)imide).^[34] The use of solvents with an intermediate polarity such as dibromomethane (DBM) for

1. Introduction

As conventional lithium-ion battery (LIB) technologies have reached their technical limits in terms of safety and energy density, all-solid-state Li or Li-ion batteries (ASLBs) using inorganic solid electrolytes (SEs) are considered as a breakthrough.^[1–13] The prerequisite of Li^+ conductivities of $\geq 10^{-3} \text{ S cm}^{-1}$ for room-temperature operable ASLBs narrows the existing candidate range of SE materials to several

K. T. Kim, Dr. D. Y. Oh, S. Jun, Y. B. Song, T. Y. Kwon, Y. Han, Prof. Y. S. Jung
Department of Chemical and Biomolecular Engineering
Yonsei University
Seoul 03722, South Korea
E-mail: yoonsjung@yonsei.ac.kr
T. Y. Kwon, Y. Han
Department of Energy Engineering
Hanyang University
Seoul 04736, South Korea

 The ORCID identification number(s) for the author(s) of this article can be found under <https://doi.org/10.1002/aenm.202003766>.

DOI: 10.1002/aenm.202003766

ASLB slurries allowed for the accommodation of sulfide SEs and SILs together, without a side reaction or phase separation; further, the electrochemical performances of the ASLBs were improved by the use of SIL-based Li^+ conductive binders, such as NBR-Li(G3)TFSI (NBR: nitrile-butadiene rubber). Despite the ionic-liquid-like behavior of the SIL itself, the thermal stability of the ASLBs appeared to have been degraded by the use of Li(G3)TFSI (Figure S1, Supporting Information). This may arise due to a complex chemical interaction between the SIL and sulfide SEs, which is accelerated at elevated temperature,^[34,39,42] thus calling for further research to upgrade slurry-fabricable Li^+ -conductive binders such that they are thermally stable. The removal of any liquid components, such as glyme, and thus, the development of dry polymer electrolyte (DPE)-based binders, could be a plausible solution to overcome the trade-off between the conducting and mechanical properties.

NBR has been the most popular binder for sulfide-based ASLBs, owing to its favorable mechanical attributes (i.e., good adhesion, rubbery property) and its solubility in sulfide-compatible solvents (e.g., xylene).^[43–49] For the preparation of DPE-type binders, however, the use of more-polar solvents is necessary, as they can dissolve Li salts such as LiTFSI, but counteract the dissolution of NBR. This complication led us to develop a new slurry fabrication protocol employing cosolvents, in which two solvent molecules work in synergy for the dissolution of NBR and LiTFSI, while being benign toward the dissolution of sulfide SE $\text{Li}_6\text{PS}_5\text{Cl}_{0.5}\text{Br}_{0.5}$ (LPSX). Moreover, it is shown that the dispersion of polymers can be controlled by the ratio of solvents in cosolvents, which results in varying electrochemical performances of the ASLBs.

2. Results and Discussion

Binary cosolvents for the slurry-fabricable DPE-type binder NBR-LiTFSI were designed by choosing each solvent such that they can dissolve either NBR or LiTFSI well, while preserving LPSX. DBM and hexyl butyrate (HB) were thus selected as the cosolvents, and exhibited no phase separation (Figure S2, Supporting Information).

For the systematic assessment of the compatibility of the processing solvents toward LPSX, the Li^+ conductivities of LPSX at 30 °C were measured after exposure to the DBM, HB, and cyclopentanone solvents at 150 °C for 6 h (Figure 1a). The corresponding X-ray diffraction (XRD) patterns and Arrhenius plots of the Li^+ conductivities are also provided in Figure S3, Supporting Information. The trend in Li^+ conductivities is consistent with that in dipole moments, that is, the lower the dipole moment, the lesser the degradation in the Li^+ conductivity. With DBM, a marginal degradation in the Li^+ conductivity was obtained (from 4.6 to 3.0 mS cm^{-1}), which is due to the absence of any nucleophilic sites. In sharp contrast, exposure to cyclopentanone resulted in the highest dipole moment, thereby significantly decreasing the Li^+ conductivity ($1.1 \times 10^{-7} \text{ S cm}^{-1}$), indicating a severe side reaction related to nucleophilic attack from the ketone group possessing lone-pair electrons at the electronegative oxygen.^[34,50] Interestingly, the degradation in Li^+ conductivity after exposure to HB was insignificant (1.8 mS cm^{-1}) despite the presence of an ester group. This result could be attributed to steric hindrance by the bulky hexyl group.^[34] Consistently, the XRD results showed that the argyrodite crystal structure was retained without the evolution of

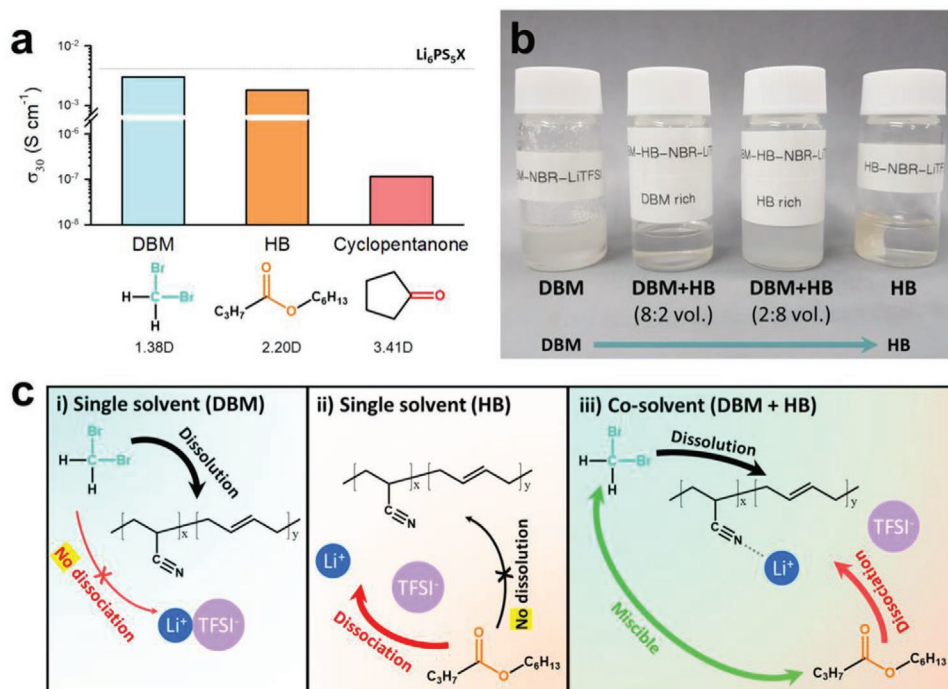


Figure 1. Compatibility of slurry-processable solvents with sulfide SE LPSX ($\text{Li}_6\text{PS}_5\text{Cl}_{0.5}\text{Br}_{0.5}$) and polymeric binder NBR. a) Li^+ conductivities of LPSX at 30 °C after exposure to DBM, HB, and cyclopentanone solvents. Dipole moments of the solvents are also shown. b) Photograph of mixtures of slurry-processable solvents (DBM, HB, or DBM+HB cosolvents), NBR, and LiTFSI. c) Schematic illustrating interactions of slurry-processable solvents with Li salt LiTFSI and binder NBR. Note that DBM and HB are miscible, and the resulting cosolvent enables the dissolution of both NBR and LiTFSI.

any impurity phases after exposure to DBM or HB (Figure S3a, Supporting Information).

Figure 1b shows photographs of mixtures of NBR, LiTFSI, and solvents, with varying ratios of DBM to HB. When using pure DBM and HB, LiTFSI (solid precipitates) and NBR (solid lump) remained undissolved, respectively. In contrast, mixtures using cosolvents of DBM and HB (hereafter referred to as “DBM+HB”) were homogeneous, although the mixture solution with a higher HB fraction (DBM:HB = 2:8) was turbid. This result is comprehensively explained in Figure 1c. Although DBM could dissolve NBR, its polarity was not high enough to dissociate LiTFSI. The use of the more-polar solvent, HB, enabled the dissociation of LiTFSI, but at the expense of the dissolving ability for NBR. The use of their blends allowed for the dissolution of both, NBR and LiTFSI, forming a homogeneous solution. In short, the results thus far confirm the suitability of DBM+HB cosolvents for a slurry containing a DPE-type binder (NBR-LiTFSI) and sulfide SEs.

Prior to the electrochemical characterization of NBR-LiTFSI processed using DBM+HB cosolvents, the effects of the cosolvent composition on the phase evolution of the ternary system, NBR-DBM-HB, and the corresponding electrochemical performance of the ASLBs, were investigated (Figure 2). Figure 2a shows the ternary diagram and photographs of four samples with varying DBM-to-HB ratios (1:0, 8:2, 5:5, and 2:8 vol). The mixture solutions appeared transparent for a DBM-to-HB ratio up to 5:5. In contrast, the solution with the highest HB fraction (80 vol%) was turbid, although no precipitation occurred after storing for several days. The addition of HB, which is an antisolvent for NBR, would cause aggregation of the polymer chains of NBR at the nanoscale,^[51,52] and scattering by visible light would become evident. In order to understand the microstructural evolution of NBR in the cosolvents, dynamic light scattering experiments were performed using the NBR-DBM-HB samples, and the results are shown in Figure 2b, Figure S4, and Table S1, Supporting Information. NBR in pure DBM showed a single peak in the particle size distribution with an average size of 30 μm (Figure S4, Supporting Information).^[52] The addition of the antisolvent HB resulted in the evolution of much smaller sized domains (hundreds of nanometers), and eventually, NBR in DBM+HB with the highest HB fraction (80 vol %) presented a single peak with the smallest average size of 382 nm. In short summary, as the HB fraction was increased, the average diameter of NBR in cosolvents decreased significantly, which indicates that the polymeric domains were aggregated with the addition of HB.^[53,54]

The schematic in Figure 2c illustrates the corresponding dispersion of the NBR polymer chains in cosolvents. In pure DBM, the NBR polymer chains are fully disentangled. As more HB is added, the disentanglement of the NBR polymer chains lessens. In other words, the NBR polymer chains are more tangled with each other (or aggregated more). This result implies that the ratio of cosolvents could affect the degree of dispersion of polymeric binders in composite electrodes, and in turn, the electrochemical performances of ASLBs. Specifically, the larger polymeric domains for using the lower fraction of HB would occupy a larger interfacial area when composite electrodes are formed from slurries. In this regard, the aggregation of polymeric domains upon increasing the fraction of HB in the cosolvents is considered beneficial for minimizing the disruption of Li⁺ contacts by polymeric binders in

all-solid-state electrodes. To visualize the spatial distribution of binders, affected by the HB fraction in cosolvents, control experiments using time-of-flight secondary ion mass spectrometry (TOFSIMS) measurements were carried out. LPSX-NBR (5 wt% NBR) composite samples were prepared using cosolvents with three different DBM-to-HB ratios; 1:0, 5:5, and 2:8 vol, and TOFSIMS maps for the CN⁻ signal were obtained (Figure S5, Supporting Information). The distribution of the CN⁻ signal became more uneven as more HB was added into DBM, confirming the more aggregated (or localized) domains of NBR via the use of antisolvent HB.

Two Li[Ni_{0.70}Co_{0.15}Mn_{0.15}]O₂ (NCM) electrodes fabricated using the conventional Li⁺-insulating binder, NBR, with an identical composition (NCM:LPSX:NBR:Super C65 = 70.0:27.5:1.5:1.0 (weight ratio)), were fabricated from the slurries using cosolvents with different DBM-to-HB volume ratios of 5:5 and 2:8. The prepared electrodes did not show any cracks or delamination (Figure S6a,b, Supporting Information). Their electrochemical performances in NCM/Li-In all-solid-state half cells at 30 °C are shown in Figure 2d,e. Compared to the case using DBM+HB in a ratio of 5:5, NCM electrodes derived from DBM+HB in a ratio of 2:8 showed remarkably improved capacities (e.g., 132 vs 119 mA h g⁻¹ at 0.2C). The transient charge-discharge voltage profiles obtained by the galvanostatic intermittent titration technique (GITT) for both electrodes and the corresponding polarization curves also confirm the faster kinetics when using the 2:8 ratio of DBM+HB than 5:5 (Figure S7, Supporting Information). Moreover, the surface coverage of NCM by the SEs, obtained by comparing results from the GITT and N₂ adsorption-desorption isotherm, was significantly higher for a higher HB fraction (2:8 vol, 24.8%), compared to the case with a lower HB fraction (5:5 vol, 11.0%) (the detailed procedure is described in the Supporting Information), which is consistent with the results in Figure 2d,e. These results are comprehensively illustrated in Figure 2f,g. For the slurry from the transparent DBM+HB with a 5:5 ratio, the NBR polymer chains were highly dispersed throughout the interfaces of NCM and LPSX, severely obstructing interfacial Li⁺ transport (Figure 2f). In contrast, with greater inclusion of the antisolvent HB (DBM:HB = 2:8 vol), the NBR polymer chains become more tangled (or aggregated), and NCM/LPSX interfacial contacts are disturbed less by the insulating NBR domain (Figure 2g).

The ratio of the DBM+HB cosolvents was thus set to 2:8 vol for preparing the slurries targeting the DPE-type binder, NBR-LiTFSI. In order to evaluate Li⁺ transport at LPSX/NBR-LiTFSI interfaces, LPSX-NBR-LiTFSI composite films were fabricated from slurries using the DBM+HB cosolvents and sandwiched by ⁶Li metal (Figure 3a). The as-prepared composites clearly showed characteristic peaks for LPSX at ≈2.3 ppm and NBR-LiTFSI at ≈-0.1 ppm without any impurity signals in magic-angle spinning (MAS) ⁶Li nuclear magnetic resonance (NMR) spectra (Figure S8, Supporting Information). After repeated cycling of ⁶Li/LPSX-NBR-LiTFSI/⁶Li symmetric cells at a constant current of 50 μA (Figure S9, Supporting Information), the LPSX-NBR-LiTFSI layer was collected and subjected to MAS ⁶Li NMR measurement (Figure 3b). The fitted results of MAS ⁶Li NMR are summarized in Table S2, Supporting Information. The ⁶Li chemical shift and full width at half maximum (FWHM) of both characteristic peaks remained unchanged after the repeated cycling, which indicates that the local environments of Li were preserved. Notably, the area of

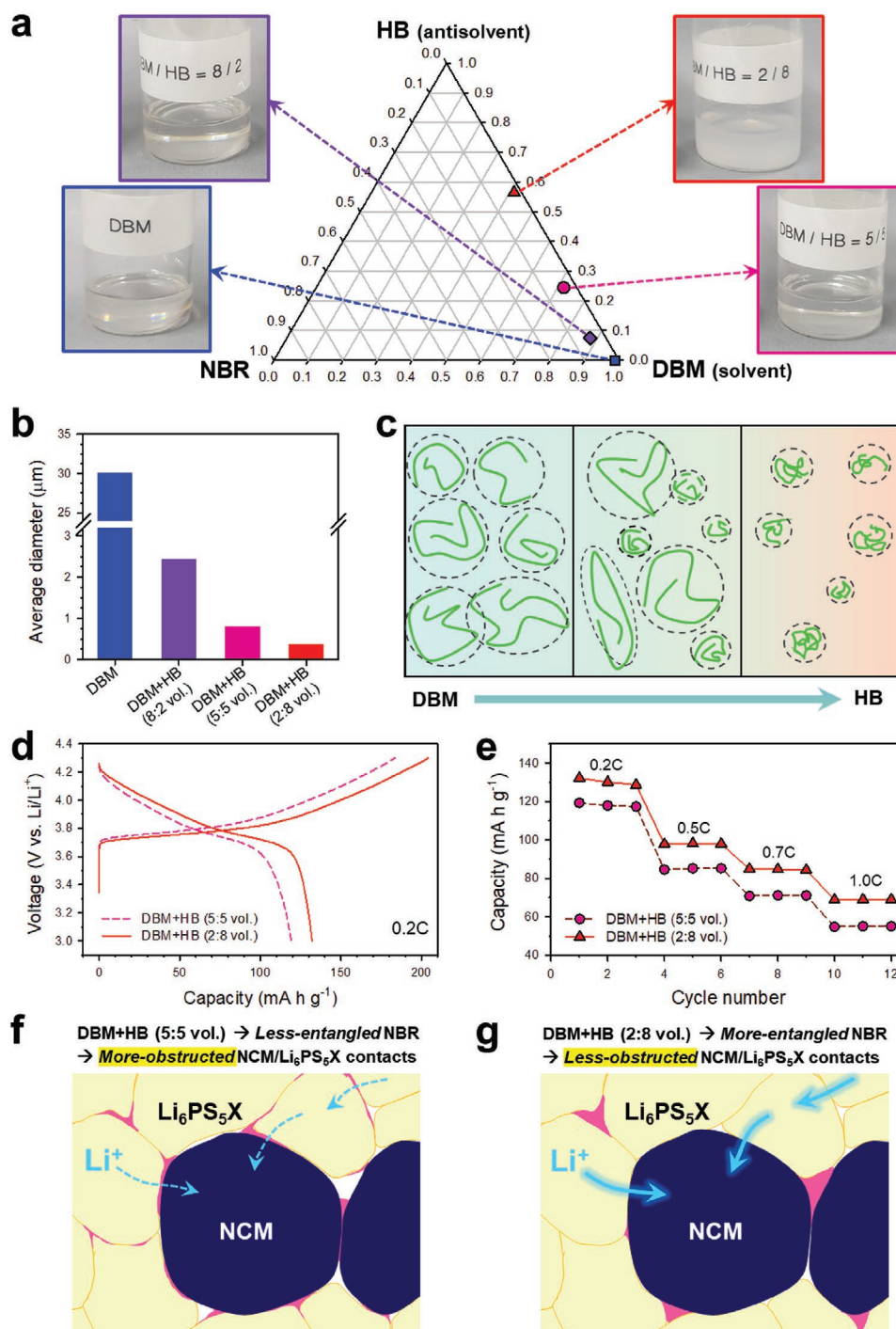


Figure 2. Cosolvent effects of NBR/(DBM+HB). a) Ternary diagram of the NBR-DBM-HB system (based on weight fraction) and corresponding photographs. Note that the mixtures appear more turbid as the fraction of the antisolvent HB is increased. b) Average diameter and c) schematic of NBR polymeric domains in cosolvents with varying compositions. d) First-cycle charge-discharge voltage profiles at 0.2C and 30 °C of NCM/Li-In all-solid-state half cells employing NCM electrodes fabricated using slurries with different compositions of DBM+HB cosolvents and e) corresponding rate capabilities. Schematic illustrating the microstructures of NCM electrodes using different cosolvents with different DBM-to-HB weight ratios of f) 5:5 and g) 2:8.

the characteristic peaks increased after the cycling, not only for the LPSX peak but also for the NBR-LiTFSI peak; by 70.4 and 18.3%, respectively. This result ensures the contribution of NBR-LiTFSI to Li⁺ transport.^[34,55] The much smaller enhancement in signals after cycling for NBR-LiTFSI, compared to

that of LPSX, is rationalized by the large difference in their Li⁺ conductivities (LPSX: $4.6 \times 10^{-3} \text{ S cm}^{-1}$ vs NBR-LiTFSI: $3.0 \times 10^{-8} \text{ S cm}^{-1}$ (Figure S10, Supporting Information)).

Sheet-type NCM electrodes employing NBR-LiTFSI were fabricated from slurries containing NCM, LPSX, Super C65, NBR,

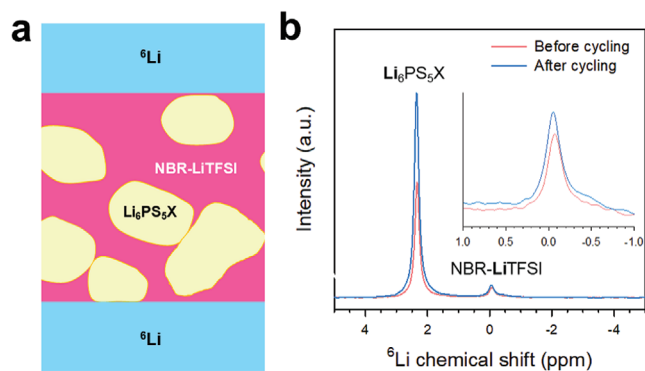


Figure 3. MAS ${}^6\text{Li}$ NMR results for ${}^6\text{Li}$ -ion non-blocking symmetric cells of ${}^6\text{Li}$ /LPSX-NBR-LiTFSI/ ${}^6\text{Li}$. a) Schematic illustration of the ${}^6\text{Li}$ /LPSX-NBR-LiTFSI/ ${}^6\text{Li}$ symmetric cells. b) MAS ${}^6\text{Li}$ NMR spectra of LPSX-NBR-LiTFSI before and after cycling.

and LiTFSI, via the use of DBM+HB cosolvents. To ensure the complete removal of any residual solvents, the electrodes were dried at as high as $150\text{ }^\circ\text{C}$. Notably, at this high temperature, the DPE binder NBR-LiTFSI remains intact, which is in contrast to the behavior of gel-type polymer electrolytes.^[56–59] The electrode composition of NCM, LPSX, Super C65, NBR, and LiTFSI was 70.0: (27.5- x): 1.0: 1.5: x (weight ratio), where x was

varied from 0.0 to 1.0 and 3.0 wt%. The NCM electrodes fabricated using the DPE binder NBR-LiTFSI did not show any delamination (Figure S6c, Supporting Information). A cross-sectional field emission scanning electron microscopy (FESEM) image of the prepared NCM electrodes shows good distribution of the electrode components (Figure S11, Supporting Information). X-ray photoelectron spectroscopy (XPS) results for the electrodes revealed the oxidized species that should be derived via the reaction with slurry solvents (Figure S12, Supporting Information).

Nyquist plots of the electron-blocking Li-In/LPSX/electrode/LPSX/Li-In symmetric cells and corresponding Li^+ conductivities of the NCM electrodes as a function of the weight fraction of LiTFSI are shown in Figure 4a,b, respectively. Two distinct semicircles may indicate different Li^+ dynamics depending on interfacial characteristics, which is an interesting topic for further study.^[60,61] The Li^+ and e^- conductivities of the electrodes are also summarized in Table S3, Supporting Information. Despite the low Li^+ conductivity of NBR-LiTFSI ($3.0 \times 10^{-8}\text{ S cm}^{-1}$), NCM electrodes containing LiTFSI showed higher Li^+ conductivities (2.2×10^{-4} and $1.8 \times 10^{-4}\text{ S cm}^{-1}$ for 1.0 and 3.0 wt% LiTFSI, respectively), compared to those without LiTFSI ($9.0 \times 10^{-5}\text{ S cm}^{-1}$). This result confirms that Li^+ transport in electrodes was facilitated by NBR-LiTFSI, which is also supported by the MAS ${}^6\text{Li}$ NMR results (Figure 3).

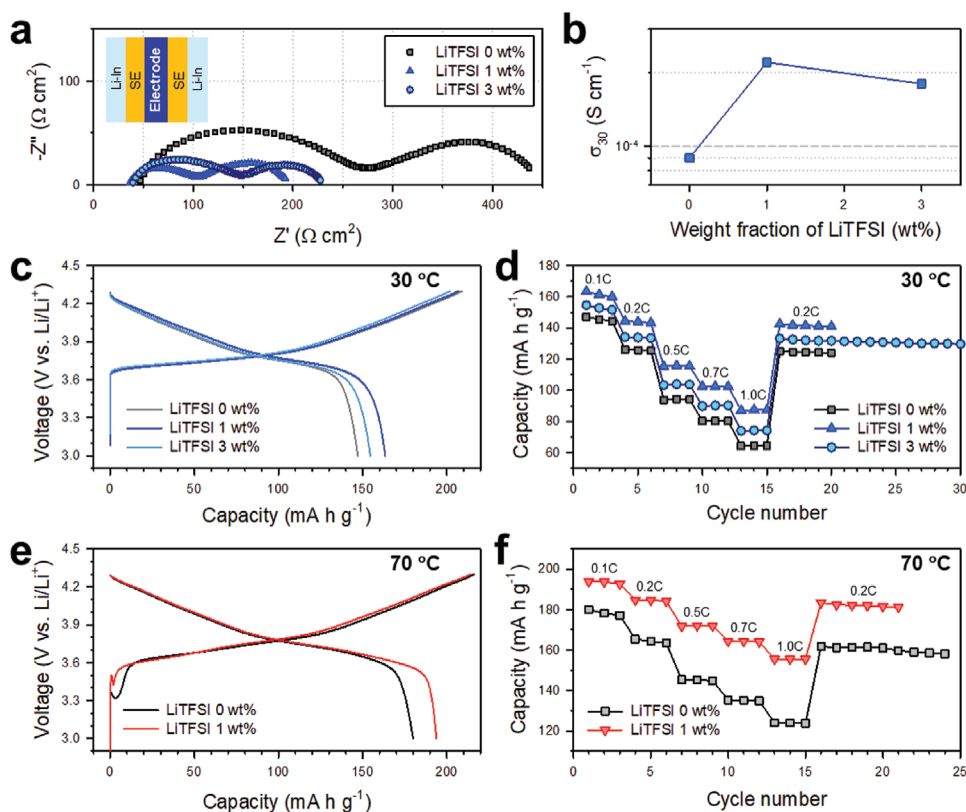


Figure 4. Comparative electrochemical characterization of slurry-fabricated sheet-type NCM electrodes fabricated using binders with varying amounts of added LiTFSI. a) Nyquist plots of e^- -blocking Li-In/LPSX/electrode/LPSX/Li-In symmetric cells containing NCM electrodes with varying amounts of LiTFSI and b) corresponding Li^+ conductivities. c) First-cycle charge-discharge voltage profiles of NCM/Li-In half cells at 0.1C and $30\text{ }^\circ\text{C}$ of NCM electrodes with varying amounts of LiTFSI and d) corresponding rate capabilities. e) First-cycle charge-discharge voltage profiles of NCM/Li-In half cells at 0.1C and $70\text{ }^\circ\text{C}$ for NCM electrodes containing varying amounts of LiTFSI and f) corresponding rate capabilities.

It is noted that the increase of the weight fraction of LiTFSI from 1.0 to 3.0 wt% didn't lead to a further increase in Li⁺ conductivity but resulted in the slightly decreased Li⁺ conductivity. This result is consistent with the Li⁺ conductivity results of NBR-LiTFSI with two different weight ratios of NBR to LiTFSI (3:2 vs 1:2, Figure S10, Supporting Information). The NBR to LiTFSI weight ratio for the electrodes containing 3 wt% LiTFSI was 1:2, and the corresponding Li⁺ conductivity was lower, as compared to NBR-LiTFSI with the weight ratio of 3:2. Moreover, the electrodes containing the higher weight fraction of LiTFSI include the correspondingly lower fraction of highly conductive LPSX: 26.5 and 23.5 wt% for the electrodes containing 1.0 and 3.0 wt% LiTFSI, respectively. The slightly decreased Li⁺ conductivity for the electrodes containing 3.0 wt% LiTFSI, compared to the electrodes with 1.0 wt% LiTFSI, is thus understood.

The advantage of the enhanced Li⁺ contact by NBR-LiTFSI was evaluated by testing NCM/Li-In half cells employing NCM electrodes tailored using NBR-LiTFSI with varying amounts of LiTFSI. The first-cycle charge-discharge voltage profiles of the NCM electrodes with 0, 1, and 3 wt% of LiTFSI at 0.1C and 30 °C are displayed in Figure 4c. With the addition of 1 wt% LiTFSI, the reversible capacity increased from 147 to 163 mA h g⁻¹, and the initial coulombic efficiency (ICE) was also enhanced from 70.4 to 78.9% (Table 1). A further increase in the amount of LiTFSI to 3 wt% resulted in a slight degradation, that is, the reversible capacity was 155 mA h g⁻¹ and ICE was 76.5%. This trend holds for the rate capability results shown in Figure 4d, and is also consistent with the overpotential obtained by GITT measurements (Figure S13, Supporting Information) and Li⁺ conductivities of the electrodes (Figure 4b). Furthermore, NBR-LiTFSI retained its functionality at as high as 70 °C (Figure 4e,f). As compared to NCM electrodes fabricated using insulating NBR (without LiTFSI), the reversible capacity and ICE increased from 180 to 194 mA h g⁻¹ and from 83.2 to 90.5%, respectively, by the application of NBR-LiTFSI.

The results thus far can be unambiguously attributed to the improved Li⁺ contact enabled by NBR-LiTFSI.^[11,25,34,50,62,63] The fact that the “soft” NBR-LiTFSI might regulate to maintain Li⁺ contact, counteracting electrochemo-mechanical degradations at the interfaces, is not ruled out.^[64,65] Moreover, NBR-LiTFSI can be used in a graphite (Gr) anode. A slight enhancement in the capacity of Gr electrodes by the application of NBR-LiTFSI is confirmed (Figure S14, Supporting Information). This result

Table 1. Electrochemical performances of sheet-type electrodes in half cells.

Electrode	Operating temperature	Fraction of LiTFSI [wt%]	Initial capacity [mA h g ⁻¹]		ICE [%]
			Charge	Discharge	
NCM	30 °C	0	209	147	70.4
		1	207	163	78.9
		3	202	155	76.5
NCM	70 °C	0	216	180	83.2
		1	214	194	90.5
		3	202	155	76.5
Gr	30 °C	0	330	307	93.2
		1	341	318	93.1

is in contrast to the poor compatibility of the SIL-type binder NBR-Li(G3)TFSI with Gr,^[66] highlighting the superior functionality of the DPE-type binder.

Finally, NCM/Gr all-solid-state full cells employing electrodes and ≈100 μm-thick SE films tailored using NBR-LiTFSI were assembled and tested at 30 °C (Figure 5). Pellet-type NCM/Gr full cells showed an initial discharge capacity of 163 mA h g_{NCM}⁻¹ at 0.1C (Figure 5a), consistent with the results for the NCM/Li-In half cell. Further, 91.6% of the capacity was retained at the 100th cycle, compared with the capacity at the 3rd cycle (Figure 5b). Moreover, 15 × 20 mm² pouch-type NCM/Gr full cells fabricated by isotactic pressing showed an initial discharge capacity of 169 mA h g_{NCM}⁻¹ at 0.05C (Figure 5c), which is similar to that for pelletized cells. Cycling performances of pellet-type full cells at 0.5C and pouch-type full cells at 0.2C are also shown in Figure S15, Supporting Information. A slight capacity fading is attributed to the side reactions of

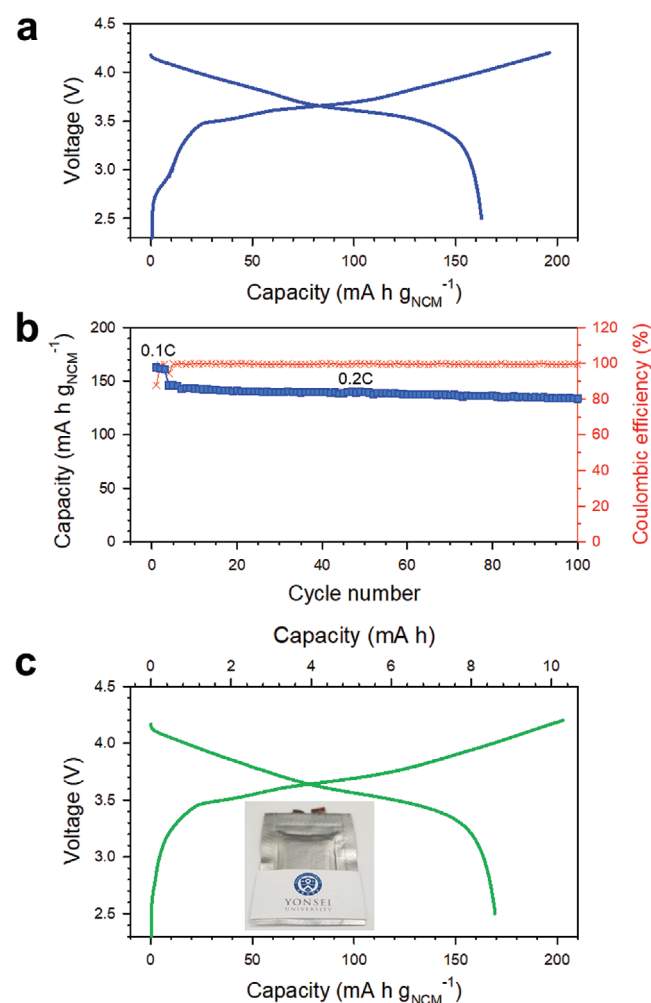


Figure 5. Results at 30 °C for NCM/Gr all-solid-state full cells employing electrodes made of a Li⁺ conductive binder (NBR-LiTFSI) using the DBM+HB cosolvent. a) First-cycle charge-discharge voltage profiles of pellet-type full cells at 0.1C and b) corresponding cycling performance. c) First-cycle charge-discharge voltage profiles of 15 × 20 mm² pouch-type full cells at 0.05C. A photograph of a pouch-type full cell is shown in the inset in panel (c).

LPSX and the (electro)chemo-mechanical effects.^[64,65,67] Ex situ XPS results (Figure S12 and Table S4, Supporting Information) showed the increased fraction of oxidized species after 100 cycles. Consistently, the EIS results for the NCM/Li-In half cells employing NCM electrodes fabricated using NBR-LiTFSI showed the increased interfacial resistance (Figure S16, Supporting Information). These results confirm the need for the development of (electro)chemical-oxidation-tolerable SE materials and interfacial engineering.^[20,67,68]

3. Conclusion

In summary, a new scalable slurry fabrication protocol using cosolvents of DBM+HB targeted at the introduction of DPE-type binders for sulfide SEs was successfully developed for practical ASLBs. The counteracting requirements for slurry solvents, that is, lower polarity for preserving vulnerable sulfide SEs and dissolving NBR but higher polarity for the dissociation of LiTFSI, could be met by blending the less-polar DBM solvent and the more-polar HB solvent. It was also demonstrated that the dispersion of the NBR binder could be controlled by adjusting the fraction of the antisolvent HB, which was confirmed by dynamic light scattering and TOFSIMS measurements. More-entangled nanoprecipitated NBR domains derived from the use of cosolvents with a higher HB fraction could thus ensure minimal obstruction of ionic contact between the electrode active materials and SEs, which resulted in enhanced electrochemical performances; to our best knowledge, this is a new finding. The MAS ⁶Li NMR and electrochemical impedance spectroscopy (EIS) measurements confirmed the facilitation of interfacial Li⁺ transport by the DPE-type binder NBR-LiTFSI derived from slurries using DBM+HB cosolvents. For sheet-type NCM electrodes tested at 30 °C, significant enhancement in the electrochemical performances, that is, increased capacities and ICEs, by the application of the cosolvent-derived NBR-LiTFSI, was confirmed. Moreover, in contrast to SIL-type binders, NBR-LiTFSI was also effective at 70 °C and in a Gr anode. Finally, the satisfactory performance of NCM/Gr full cells employing electrodes and SE films made of NBR-LiTFSI using cosolvents highlights the practicability of the new protocol. Considering that the Li⁺ conductivity of NBR-LiTFSI was low (3.0×10^{-8} S cm⁻¹), the application of alternative DPEs showing higher Li⁺ conductivities in the range of 10^{-5} – 10^{-4} S cm⁻¹ would enable further progress.^[10,69–71] Moreover, our new proof-of-concept—introducing a cosolvent, not only widens the candidate pool for slurry solvents and polymeric binders, but also provides new insight into the controllability of the dispersion of binders.

4. Experimental Section

Preparation of Materials: Argyrodite Li₆PS₅Cl_{0.5}Br_{0.5} (LPSX) was prepared by ball-milling and subsequent heat treatment under Ar atmosphere. After ball-milling a stoichiometric mixture of Li₂S (99.9%, Alfa-Aesar), P₂S₅ (99%, Sigma Aldrich), and LiCl (99.99%, Sigma Aldrich) at 600 rpm for 10 h in a ZrO₂ vial with ZrO₂ balls using the Pulverisette 7PL (Fritsch GmbH), heat treatment was carried out at 550 °C for 5 h under Ar atmosphere. The Li⁺ conductivity of the resulting powders was 4.6 mS cm⁻¹ at 30 °C. NCM (LiNi_{0.70}Co_{0.15}Mn_{0.15}O₂) powders were coated by LiNbO₃ (1.4 wt%) via a wet-chemical method using lithium ethoxide (99.95%, Sigma Aldrich) and niobium ethoxide (99.95%, Sigma Aldrich) as described in the previous report.^[62] For

the preparation of NBR/DBM-HB solutions, NBR was first dissolved into DBM (99%, Sigma Aldrich), followed by the addition of HB (98%, Sigma Aldrich). LPSX-NBR-LiTFSI (LiTFSI, 99.95%, Sigma Aldrich) composites were fabricated from the slurries prepared by dissolving targeted amounts of NBR and LiTFSI in DBM+HB cosolvents. All the liquids (DBM and HB) and solids (LiTFSI and NBR) used for the slurries were dried using molecular sieves (4 Å, DAEJUNG) and at 100 °C under vacuum, respectively.

Fabrication of Electrodes: The wet slurries consisting of active materials (NCM or Gr), LPSX, NBR, carbon additive (Super C65, only for NCM), and LiTFSI were prepared using DBM+HB cosolvents with target compositions. The electrode composition was 70:27.5-x:1.5:1:x and 60:38-x:0.2:x for the NCM and Gr electrodes, respectively. The slurry mixtures were cast on current collectors (carbon-coated Al foils for NCM and Ni foils for Gr, respectively) using the doctor-blade method, followed by heat treatment at 150 °C under vacuum.

Material Characterization: The dipole moments of the solvents were obtained using a semi-empirical method with Gaussian 09W software.^[72] For XRD measurements, the SEs were sealed with a beryllium window and mounted on a MiniFlex 600 diffractometer (Rigaku Corp.; Cu K_α radiation of 1.5406 Å) at 40 kV and 15 mA. The particle size distribution and PDI of NBR were measured using an ELSZ-1000 zeta potential and particle size analyzer (Otsuka Electronics). For MAS ⁶Li NMR spectroscopy, samples were collected from the LPSX-NBR-LiTFSI layer in ⁶Li/LPSX-NBR-LiTFSI/⁶Li cells and analyzed using a AVANCE III 400 (Bruker) at a resonance frequency of 58.883 MHz and a spinning rate of 10 kHz. The chemical shift was referenced to LiCl at 0 ppm and a spinning rate of 10 kHz. The fitting of ⁶Li NMR spectra was conducted using MestReNova software. Cross-sectioned NCM electrode samples were obtained by polishing at 6 kV for 6 h, followed by 4 kV for 3 h with an Ar ion beam (JEOL, IB19510CP). The corresponding FESEM images were obtained using the AURIGA (Carl Zeiss). For the TOFSIMS experiments, LPSX-NBR composite samples (95:5 weight ratio) were prepared using cosolvent with three different DBM-to-HB ratios; 1:0, 5:5, and 2:8 vol TOFSIMS measurements were performed using a TOFSIMS.5 instrument (ION-TOF) equipped with a 30 keV Bi cluster primary-ion gun for analysis. Bi³⁺ ions with an energy of 30 keV were used as primary-ion species and the $10 \times 10 \mu\text{m}^2$ or $5 \times 5 \mu\text{m}^2$ analysis area were rasterized. The ex situ XPS measurements were carried out with a monochromatic Al K_α source (1486.6 eV) at 12 kV and 6 mA using K-Alpha+ (Thermo Fisher Scientific). Samples were mounted on a sample holder in an Ar-filled glove box and transferred into the XPS equipment without any exposure to air.

Electrochemical Characterization: The Li-In (nominal composition: Li_{0.5}In) as the counter and reference electrodes were prepared by ball-milling In (Sigma Aldrich, 99%) and Li (FMC Lithium Corp.) powders. To fabricate the NCM (or Gr)/Li-In half-cells, the electrodes and Li-In electrodes were placed on each side of the pre-pelletized LPSX layers (150 mg), and pelletized at 370 MPa at room temperature. Galvanostatic charge-discharge cycling tests were carried out at 30 or 70 °C between 3.0 and 4.3 V (vs Li/Li⁺) for NCM or 0.005 and 2.000 V (vs Li/Li⁺) for Gr. To fabricate NCM/Gr full cells, the SE layers were coated directly on the as-formed Gr electrodes by the doctor-blade method using LPSX-NBR-(DBM+HB) slurries. The thickness of the SE layers was ≈100 μm. The resulting assemblies were cold-pressed at 370 MPa. For pouch-type cells, isotactic pressing was conducted. Galvanostatic charge-discharge cycling tests for the full cells were carried out at 30 °C between 3.0 and 4.2 V. The EIS data were collected with an amplitude of 14.1 mV and frequency range from 1 Hz to 7 MHz using an Iviumstat (IVIUM Technologies Corp.). The GITT measurements were carried out with a pulse current of 0.5C for 60 s and rest for 2 h. For tracking Li⁺ pathways, ⁶Li⁺-ion nonblocking symmetric cells of ⁶Li/LPSX-NBR-LiTFSI/⁶Li were assembled as follows. ⁶Li foils were prepared by compressing ⁶Li chunks (95%, Sigma Aldrich). The ⁶Li/LPSX-NBR-LiTFSI/⁶Li cells were cycled at 50 μA cm⁻² at each cycle for 2 h at 70 °C. All procedures related to the fabrication of the all-solid-state cells were performed in a polyaryletheretherketone (PEEK) mold (1.3 cm²) with two Ti metal rods. The all-solid-state cells except for the pouch-type cells were tested under ≈70 MPa. The pouch-type cells were tested without external pressure.

Supporting Information

Supporting Information is available from the Wiley Online Library or from the author.

Acknowledgements

This work was supported by Hyundai Motors, by the Technology Development Program to Solve Climate Changes and by the Basic Science Research Program through the National Research Foundation of Korea (NRF) funded by the Ministry of Science, ICT & Future Planning (NRF2017M1A2A2044501 and NRF-2018R1A2B6004996), and by the Materials and Components Technology Development Program of MOTIE/KEIT (10077709 and 20012216). The work was also funded by the Yonsei University Research Fund of 2020 (2020-22-0531). Yonsei University Research Funding added to acknowledgements on May 6, 2021.

Conflict of Interest

The authors declare no conflict of interest.

Data Availability Statement

Research data are not shared.

Keywords

electrodes, Li⁺-conductive polymeric binders, slurry processes, solid electrolytes, solid-state batteries

Received: December 4, 2020

Revised: February 19, 2021

Published online: March 14, 2021

- [1] Y. Kato, S. Hori, T. Saito, K. Suzuki, M. Hirayama, A. Mitsui, M. Yonemura, H. Iba, R. Kanno, *Nat. Energy* **2016**, *1*, 16030.
- [2] J. Janek, W. G. Zeier, *Nat. Energy* **2016**, *1*, 16141.
- [3] X. Han, Y. Gong, K. Fu, X. He, G. T. Hitz, J. Dai, A. Pearse, B. Liu, H. Wang, G. Rubloff, Y. Mo, V. Thangadurai, E. D. Wachsman, L. Hu, *Nat. Mater.* **2017**, *16*, 572.
- [4] K. H. Park, Q. Bai, D. H. Kim, D. Y. Oh, Y. Zhu, Y. Mo, Y. S. Jung, *Adv. Energy Mater.* **2018**, *8*, 1800035.
- [5] A. Manthiram, X. Yu, S. Wang, *Nat. Rev. Mater.* **2017**, *2*, 16103.
- [6] Z. Zhang, Y. Shao, B. Lotsch, Y.-S. Hu, H. Li, J. Janek, L. F. Nazar, C.-W. Nan, J. Maier, M. Armand, L. Chen, *Energy Environ. Sci.* **2018**, *11*, 1945.
- [7] T. Famprakis, P. Canepa, J. A. Dawson, M. S. Islam, C. Masquelier, *Nat. Mater.* **2019**, *18*, 1278.
- [8] F. Han, A. S. Westover, J. Yue, X. Fan, F. Wang, M. Chi, D. N. Leonard, N. J. Dudney, H. Wang, C. Wang, *Nat. Energy* **2019**, *4*, 187.
- [9] M. J. Wang, R. Choudhury, J. Sakamoto, *Joule* **2019**, *3*, 2165.
- [10] R. Chen, Q. Li, X. Yu, L. Chen, H. Li, *Chem. Rev.* **2020**, *120*, 6820.
- [11] A. Banerjee, K. H. Park, J. W. Heo, Y. J. Nam, C. K. Moon, S. M. Oh, S.-T. Hong, Y. S. Jung, *Angew. Chem., Int. Ed.* **2016**, *55*, 9634.
- [12] L. Duchêne, A. Remhof, H. Hagemann, C. Battaglia, *Energy Storage Mater.* **2020**, *25*, 782.
- [13] Q. Zhang, D. Cao, Y. Ma, A. Natan, P. Aurora, H. Zhu, *Adv. Mater.* **2019**, *31*, 1901131.
- [14] H.-J. Deiseroth, S.-T. Kong, H. Eckert, J. Vannahme, C. Reiner, T. Zaiß, M. Schlosser, *Angew. Chem., Int. Ed.* **2008**, *47*, 755.
- [15] P. Adeli, J. D. Bazak, K. H. Park, I. Kochetkov, A. Huq, G. R. Goward, L. F. Nazar, *Angew. Chem., Int. Ed.* **2019**, *58*, 8681.
- [16] R. Murugan, V. Thangadurai, W. Weppner, *Angew. Chem., Int. Ed.* **2007**, *46*, 7778.
- [17] S. Kim, H. Oguchi, N. Toyama, T. Sato, S. Takagi, T. Otomo, D. Arunkumar, N. Kuwata, J. Kawamura, S.-i. Orimo, *Nat. Commun.* **2019**, *10*, 1081.
- [18] T. Asano, A. Sakai, S. Ouchi, M. Sakaida, A. Miyazaki, S. Hasegawa, *Adv. Mater.* **2018**, *30*, 1803075.
- [19] X. Li, J. Liang, X. Yang, K. R. Adair, C. Wang, F. Zhao, X. Sun, *Energy Environ. Sci.* **2020**, *13*, 1429.
- [20] H. Kwak, D. Han, J. Lyoo, J. Park, S. H. Jung, Y. Han, G. Kwon, H. Kim, S.-T. Hong, K.-W. Nam, Y. S. Jung, *Adv. Energy Mater.* **2021**, 2003190.
- [21] J. Awaka, N. Kijima, H. Hayakawa, J. Akimoto, *J. Solid State Chem.* **2009**, *182*, 2046.
- [22] N. Kamaya, K. Homma, Y. Yamakawa, M. Hirayama, R. Kanno, M. Yonemura, T. Kamiyama, Y. Kato, S. Hama, K. Kawamoto, A. Mitsui, *Nat. Mater.* **2011**, *10*, 682.
- [23] A. Sakuda, A. Hayashi, M. Tatsumisago, *Sci. Rep.* **2013**, *3*, 2261.
- [24] Y. J. Nam, S.-J. Cho, D. Y. Oh, J.-M. Lim, S. Y. Kim, J. H. Song, Y.-G. Lee, S.-Y. Lee, Y. S. Jung, *Nano Lett.* **2015**, *15*, 3317.
- [25] D. H. Kim, D. Y. Oh, K. H. Park, Y. E. Choi, Y. J. Nam, H. A. Lee, S.-M. Lee, Y. S. Jung, *Nano Lett.* **2017**, *17*, 3013.
- [26] D. Y. Oh, D. H. Kim, S. H. Jung, J.-G. Han, N.-S. Choi, Y. S. Jung, *J. Mater. Chem. A* **2017**, *5*, 20771.
- [27] Y. J. Nam, D. Y. Oh, S. H. Jung, Y. S. Jung, *J. Power Sources* **2018**, *375*, 93.
- [28] Y. J. Nam, K. H. Park, D. Y. Oh, W. H. An, Y. S. Jung, *J. Mater. Chem. A* **2018**, *6*, 14867.
- [29] D. H. Kim, H. A. Lee, Y. B. Song, J. W. Park, S.-M. Lee, Y. S. Jung, *J. Power Sources* **2019**, *426*, 143.
- [30] M. Yamamoto, Y. Terauchi, A. Sakuda, M. Takahashi, *J. Power Sources* **2018**, *402*, 506.
- [31] K. Lee, J. Lee, S. Choi, K. Char, J. W. Choi, *ACS Energy Lett.* **2019**, *4*, 94.
- [32] N. Dunlap, J. Kim, K. H. Oh, S.-H. Lee, *J. Electrochem. Soc.* **2019**, *166*, A915.
- [33] D. H. Kim, Y.-H. Lee, Y. B. Song, H. Kwak, S.-Y. Lee, Y. S. Jung, *ACS Energy Lett.* **2020**, *5*, 718.
- [34] D. Y. Oh, Y. J. Nam, K. H. Park, S. H. Jung, K. T. Kim, A. R. Ha, Y. S. Jung, *Adv. Energy Mater.* **2019**, *9*, 1802927.
- [35] J. Schnell, T. Günther, T. Knoche, C. Vieider, L. Köhler, A. Just, M. Keller, S. Passerini, G. Reinhart, *J. Power Sources* **2018**, *382*, 160.
- [36] A. Bielefeld, D. A. Weber, J. Janek, *ACS Appl. Mater. Interfaces* **2020**, *12*, 12821.
- [37] S. Jun, Y. J. Nam, H. Kwak, K. T. Kim, D. Y. Oh, Y. S. Jung, *Adv. Funct. Mater.* **2020**, *30*, 2002535.
- [38] D. H. S. Tan, A. Banerjee, Z. Deng, E. A. Wu, H. Nguyen, J.-M. Doux, X. Wang, J.-h. Cheng, S. P. Ong, Y. S. Meng, Z. Chen, *ACS Appl. Energy Mater.* **2019**, *2*, 6542.
- [39] M. Yamamoto, Y. Terauchi, A. Sakuda, M. Takahashi, *Sci. Rep.* **2018**, *8*, 1212.
- [40] F. Hippauf, B. Schumm, S. Doerfler, H. Althues, S. Fujiki, T. Shiratsuchi, T. Tsujimura, Y. Aihara, S. Kaskel, *Energy Storage Mater.* **2019**, *21*, 390.
- [41] Y.-G. Lee, S. Fujiki, C. Jung, N. Suzuki, N. Yashiro, R. Omoda, D.-S. Ko, T. Shiratsuchi, T. Sugimoto, S. Ryu, J. H. Ku, T. Watanabe, Y. Park, Y. Aihara, D. Im, I. T. Han, *Nat. Energy* **2020**, *5*, 299.
- [42] S. Tsuzuki, W. Shinoda, M. Matsugami, Y. Umeyayashi, K. Ueno, T. Mandai, S. Seki, K. Dokko, M. Watanabe, *Phys. Chem. Chem. Phys.* **2015**, *17*, 126.
- [43] K. Lee, S. Kim, J. Park, S. H. Park, A. Coskun, D. S. Jung, W. Cho, J. W. Choi, *J. Electrochem. Soc.* **2017**, *164*, A2075.
- [44] A. Sakuda, K. Kuratani, M. Yamamoto, M. Takahashi, T. Takeuchi, H. Kobayashi, *J. Electrochem. Soc.* **2017**, *164*, A2474.
- [45] K. Chen, S. Shinjo, A. Sakuda, K. Yamamoto, T. Uchiyama, K. Kuratani, T. Takeuchi, Y. Orikasa, A. Hayashi, M. Tatsumisago,

- Y. Kimura, T. Nakamura, K. Amezawa, Y. Uchimoto, *J. Phys. Chem. C* **2019**, 123, 3292.
- [46] N. Riphahaus, P. Strobl, B. Stiaszny, T. Zinkevich, M. Yavuz, J. Schnell, S. Indris, H. A. Gasteiger, S. J. Sedlmaier, *J. Electrochem. Soc.* **2018**, 165, A3993.
- [47] K. Kim, J. Park, G. Jeong, J.-S. Yu, Y.-C. Kim, M.-S. Park, W. Cho, R. Kanno, *ChemSusChem* **2019**, 12, 2637.
- [48] W. Cho, J. Park, K. Kim, J.-S. Yu, G. Jeong, *Small* **2021**, 17, 1902138.
- [49] S. Ito, S. Fujiki, T. Yamada, Y. Aihara, Y. Park, T. Y. Kim, S.-W. Baek, J.-M. Lee, S. Doo, N. Machida, *J. Power Sources* **2014**, 248, 943.
- [50] D. Y. Oh, Y. J. Nam, K. H. Park, S. H. Jung, S.-J. Cho, Y. K. Kim, Y.-G. Lee, S.-Y. Lee, Y. S. Jung, *Adv. Energy Mater.* **2015**, 5, 1500865.
- [51] S. Schubert, J. J. T. Delaney, U. S. Schubert, *Soft Matter* **2011**, 7, 1581.
- [52] S. Hornig, T. Heinze, C. R. Becer, U. S. Schubert, *J. Mater. Chem.* **2009**, 19, 3838.
- [53] S. A. Khan, M. Schneider, *Macromol. Biosci.* **2013**, 13, 455.
- [54] X. Wu, Y. Chang, Y. Fu, L. Ren, J. Tong, J. Zhou, *Starch* **2016**, 68, 258.
- [55] J. Zheng, M. Tang, Y.-Y. Hu, *Angew. Chem., Int. Ed.* **2016**, 55, 12538.
- [56] X. Cheng, J. Pan, Y. Zhao, M. Liao, H. Peng, *Adv. Energy Mater.* **2018**, 8, 1702184.
- [57] S. Liang, W. Yan, X. Wu, Y. Zhang, Y. Zhu, H. Wang, Y. Wu, *Solid State Ion.* **2018**, 318, 2.
- [58] J. Chai, Z. Liu, J. Zhang, J. Sun, Z. Tian, Y. Ji, K. Tang, X. Zhou, G. Cui, *ACS Appl. Mater. Interfaces* **2017**, 9, 17897.
- [59] F.-Q. Liu, W.-P. Wang, Y.-X. Yin, S.-F. Zhang, J.-L. Shi, L. Wang, X.-D. Zhang, Y. Zheng, J.-J. Zhou, L. Li, Y.-G. Guo, *Sci. Adv.* **2018**, 4, eaat5383.
- [60] N. Kaiser, S. Spannenberger, M. Schmitt, M. Cronau, Y. Kato, B. Roling, *J. Power Sources* **2018**, 396, 175.
- [61] H. Kwak, J. Lyoo, J. Park, Y. Han, R. Asakura, A. Remhof, C. Battaglia, H. Kim, S.-T. Hong, Y. S. Jung, *Energy Storage Mater.* **2021**, 37, 47.
- [62] K. H. Park, D. Y. Oh, Y. E. Choi, Y. J. Nam, L. Han, J.-Y. Kim, H. Xin, F. Lin, S. M. Oh, Y. S. Jung, *Adv. Mater.* **2016**, 28, 1874.
- [63] F. Hao, X. Chi, Y. Liang, Y. Zhang, R. Xu, H. Guo, T. Terlier, H. Dong, K. Zhao, J. Lou, Y. Yao, *Joule* **2019**, 3, 1349.
- [64] S. H. Jung, U.-H. Kim, J.-H. Kim, S. Jun, C. S. Yoon, Y. S. Jung, Y.-K. Sun, *Adv. Energy Mater.* **2020**, 10, 1903360.
- [65] R. Koerver, I. Aygün, T. Leichtweiß, C. Dietrich, W. Zhang, J. O. Binder, P. Hartmann, W. G. Zeier, J. Janek, *Chem. Mater.* **2017**, 29, 5574.
- [66] H. Moon, R. Tatara, T. Mandai, K. Ueno, K. Yoshida, N. Tachikawa, T. Yasuda, K. Dokko, M. Watanabe, *J. Phys. Chem. C* **2014**, 118, 20246.
- [67] S. H. Jung, K. Oh, Y. J. Nam, D. Y. Oh, P. Brüner, K. Kang, Y. S. Jung, *Chem. Mater.* **2018**, 30, 8190.
- [68] Y. Xiao, L. J. Miara, Y. Wang, G. Ceder, *Joule* **2019**, 3, 1252.
- [69] J. Lopez, D. G. Mackanic, Y. Cui, Z. Bao, *Nat. Rev. Mater.* **2019**, 4, 312.
- [70] L. Yue, J. Ma, J. Zhang, J. Zhao, S. Dong, Z. Liu, G. Cui, L. Chen, *Energy Storage Mater.* **2016**, 5, 139.
- [71] L. Long, S. Wang, M. Xiao, Y. Meng, *J. Mater. Chem. A* **2016**, 4, 10038.
- [72] J. J. P. Stewart, *J. Mol. Model.* **2007**, 13, 1173.